

# A high power 2.3 $\mu\text{m}$ Yb:Tm:YLF laser diode-pumped simultaneously at 685 and 960 nm

P S F de Matos, N U Wetter, L Gomes, I M Ranieri and S L Baldochi

Centro de Lasers e Aplicações, IPEN/SP, Avenida Professor Lineu Prestes, 2242, São Paulo 05508-000, Brazil

E-mail: [nuwetter@gmail.com](mailto:nuwetter@gmail.com)

Received 5 March 2008, accepted for publication 17 April 2008

Published 27 August 2008

Online at [stacks.iop.org/JOptA/10/104009](http://stacks.iop.org/JOptA/10/104009)

## Abstract

Energy-transfer processes in a Yb:Tm:YLF laser under 685 and 960 nm pumping have been quantitatively studied and computer simulations considering the full rate-equation scheme up to the  $^1\text{G}_4$  level have been performed. The 2.3  $\mu\text{m}$  laser efficiency has been simulated under simultaneous diode pumping at both wavelengths. Optimized values of 685–960 nm pump power ratio for typical laser cavity parameters were derived to achieve maximum output power under constant pump power. Laser experiments performed at 2.3  $\mu\text{m}$  are in agreement with these results. The achieved output power of 620 mW is the highest reported so far.

**Keywords:** diode-pumped laser

## 1. Introduction

There are many application areas where tunable lasers emitting around the 2.3  $\mu\text{m}$  region are of importance. They are especially of interest in gas detection [1, 2] systems, because of the presence of strong absorption lines in the spectral region around 2.3  $\mu\text{m}$  for atmospheric pollutants such as CO, CH<sub>4</sub> and HF. The 2.3  $\mu\text{m}$  laser is used for sensing carbon monoxide and hydrocarbon gases in combustion experiments and LIDAR applications [3], in part because of its relatively weak water vapor absorption. *In situ* absorption measurements of CO concentration in combustion experiments have shown a minimum detectivity of less than 10 ppm using 2.3  $\mu\text{m}$  radiation. Lasers emitting in the region 2.0–2.5  $\mu\text{m}$  have also gained renewed interest for non-invasive blood glucose measurements [4] because of their capability to generate measurements with very high signal-to-noise ratio.

Large emission spectra around 2.3  $\mu\text{m}$  with demonstrated tuning range of 2.2–2.45  $\mu\text{m}$  can be obtained using the thulium-doped host YLF [5]. Tm:YLF has strong absorption lines at 685 and 780 nm that are accessible with diode lasers. The absorption at 685 nm is three times larger than that at 780 nm [6]. Due to a highly concentration-dependent cross-relaxation process that leads to a reduction of the 2.3  $\mu\text{m}$

emission from the upper laser level, the thulium concentration should be kept below 2 mol% [5]. For efficient pump absorption, a high concentration sensitizer like ytterbium can be used that may be pumped at 960 nm.

Three ( $K_1$ ,  $K_2$ ,  $K_3$ ) energy-transfer up-conversion (ETU) processes occur when Yb:Tm:YLF is pumped at 960 nm, as illustrated in figure 1. After pump excitation from the  $^2\text{F}_{7/2}$  level to the  $^2\text{F}_{5/2}$  level, the first ETU process,  $K_1$ , transfers energy from the ytterbium to the  $^3\text{H}_5$  thulium level, followed by a fast multi-phonon relaxation down to the metastable  $^3\text{F}_4$  level. The second ETU process,  $K_2$ , causes transfer to the  $^3\text{F}_2$  energy level of  $\text{Tm}^{3+}$  followed by a rapid relaxation to the upper laser level ( $^3\text{H}_4$ ). The third ETU process,  $K_3$ , causes losses to the system because it transfers population from the upper laser level into the  $^1\text{G}_4$  level of Tm. Other processes deplete the upper laser level: the non-radiative transfer via cross-relaxation originating from the  $^3\text{H}_4$  and  $^3\text{H}_6$  levels to the  $^3\text{F}_4$  level ( $K_4$ ) and the back-transfer ( $K_5$ ) from the  $^3\text{H}_4$  thulium level to the  $^2\text{F}_{5/2}$  ytterbium level.

In the 685 nm pumping scheme, thulium is pumped from the  $^3\text{H}_6$  ground state into the  $^3\text{F}_3$  manifold followed by a fast multi-phonon relaxation to the upper laser level  $^3\text{H}_4$ . Laser action at 2.3  $\mu\text{m}$  in Tm is based on the  $^3\text{H}_4$ – $^3\text{H}_5$  transition.

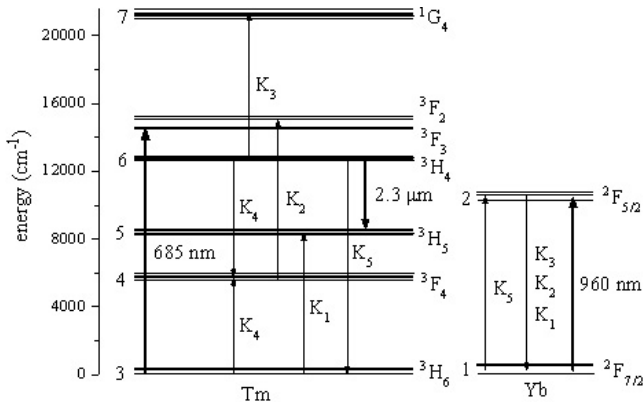


**Figure 1.** Scheme of the Yb:Yb:YLF energy levels.  $K_1, K_2, K_3$  represent energy-transfer up-conversions;  $K_4$  is a cross-relaxation and  $K_5$  a back-transfer.

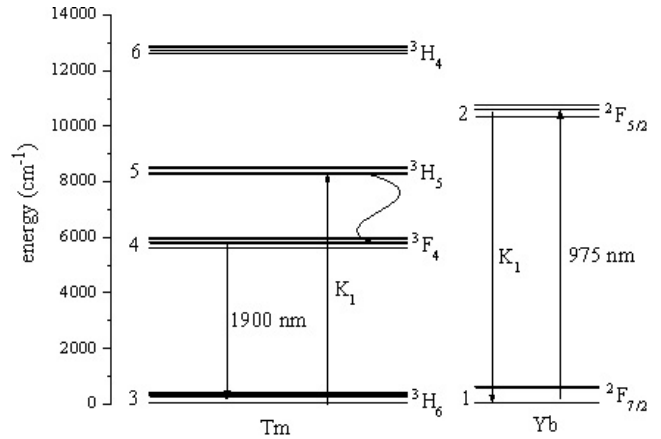


**Figure 2.** Energy levels and transfer process  $K_1$ .

In this work we demonstrate agreement between spectroscopic measurements taken at our laboratory and the simulations using a MATLAB based computer program using energy-transfer probabilities from the literature. With this program, optimized values of 685–960 nm pump power ratio for typical laser cavity parameters are calculated. The output power achieved in this experiment is the highest reported so far for the 2.3  $\mu\text{m}$  emission.

## 2. Spectroscopic measurements

The Yb:Yb:YLF crystal was grown at our in-home crystal growth facility with a concentration of  $9.44 \pm 0.06$  mol% ytterbium and  $1.15 \pm 0.02$  mol% thulium, as measured with energy dispersive x-ray fluorescence (EDXRF; Shimadzu EDX-900). These concentrations allow for maximum efficiency of the 2.3  $\mu\text{m}$  emission [7].

The experimental setup mainly comprises an optical parametric oscillator (OPO from OPOTEK) pumped by the second harmonic (532 nm) of a Nd:YAG laser (Brilliant B from Quantel), tunable in the near-infrared range from 680 to 990 nm, which delivers a typical energy of 10 mJ with a repetition rate of 10 Hz, pulse duration of 4 ns and bandwidth of 4 nm. The detection apparatus consisted of a single-grating spectrometer (25 cm monochromator from KRATOS) with an optical grating with blaze at 300 nm. The luminescence in the visible spectral region was collected perpendicularly to the laser excitation, in order to minimize the scattered laser light, with a refrigerated ( $-30^\circ\text{C}$ ) photomultiplier (S-20 type cathode from EMI, model QB-9558). For infrared measurements, an InSb detector refrigerated to liquid nitrogen temperature (77 K) was used. The luminescence decay times were recorded using a 100 mega samples per second digital oscilloscope (TDS 410 Tektronix). Acquisition was done at three different timescales (short, middle and long) in order to achieve good resolution at the beginning and at the end of the luminescence curves.

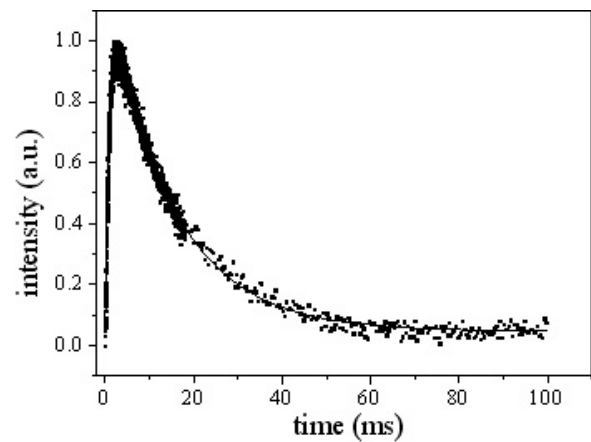


**Figure 3.** Thulium emission at 1900 nm under ytterbium excitation at 960 nm. The fitted rise time for the Yb–Tm energy transfer and the lifetime of the thulium  $^3\text{F}_4$  level are  $0.807 \pm 0.062$  ms and  $15.04 \pm 0.12$  ms, respectively.

### 2.1. First energy-transfer process

The Yb:Yb:YLF crystal was excited at 960 nm and the thulium emission was collected at 1900 nm using a filter of 10 nm band-pass. Care was taken to avoid radiation trapping by exciting the sample at the edge closest to the detection apparatus. The energy levels and transfer mechanisms involved are shown in figure 2. The measurements and the applied fit (equation (1)) are given in figure 3.

The rise time and lifetime were obtained by fitting the measured luminescence intensity curves with the following equation [8]:

$$I = A \left[ \exp\left(\frac{-t}{t_d}\right) - \exp\left(\frac{-t}{t_s}\right) \right] \quad (1)$$

where  $I$  is the signal intensity, and  $A$  its amplitude;  $t_s$  and  $t_d$  are the rise time and the decay time, respectively. The fit with a double exponential curve does not correspond to an analytical solution of rate equations, but only serves as a guide to the eye and to obtain an estimate of the energy-transfer times and lifetimes involved. It is important to remark that the measured

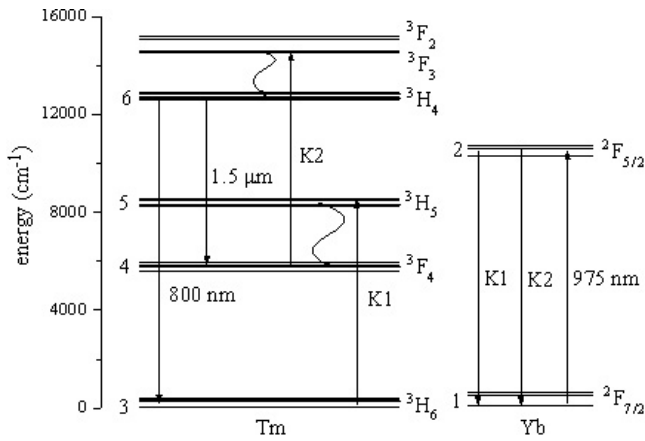


**Figure 4.** Energy-transfer processes and energy levels involved in the second-step ETU process.

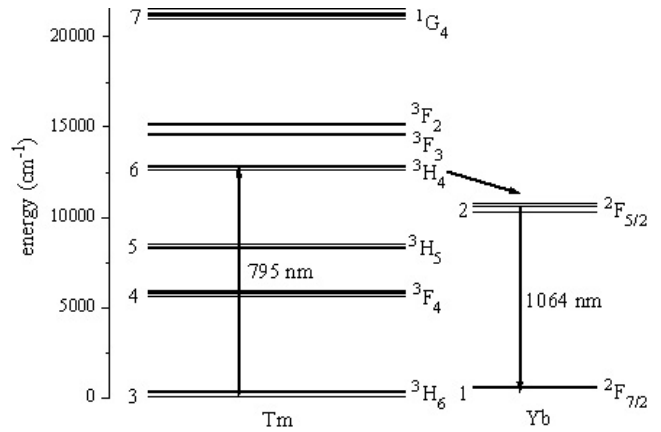


**Figure 6.** Energy-transfer processes and energy levels involved in the back-transfer process.

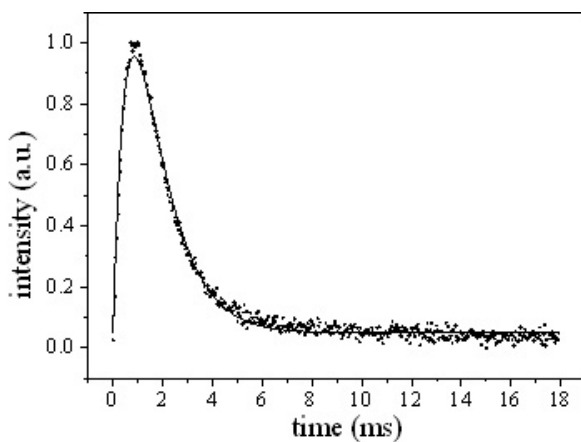


**Figure 5.** Thulium emission from the  $^3H_4$  energy level measured at 1500 nm. The pump wavelength was 975 nm. The fitted rise time for the Yb–Tm energy transfer and the lifetime of the thulium  $^3H_4$  level are  $0.65 \pm 0.26$  ms and  $1.148 \pm 0.038$  ms, respectively.

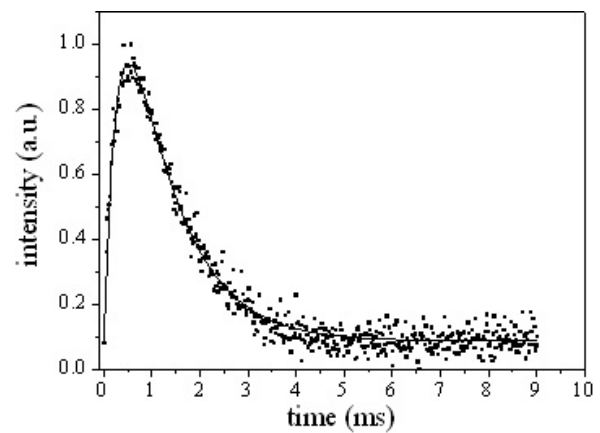


**Figure 7.** Ytterbium emission at 1064 nm under thulium excitation at 795 nm. The fitted rise time for the Tm–Yb energy transfer and the lifetime of the ytterbium  $^2F_{5/2}$  level are  $0.293 \pm 0.011$  ms and  $1.011 \pm 0.029$  ms, respectively.

rise times do not correspond to one single and isolated energy-transfer probability but to a superposition of a series of energy-transfer processes involved.

### 2.2. Second energy-transfer process

The  $^3H_4$  thulium energy level becomes populated after the second ETU process. The respective energy-transfer probability  $K_2$  depends on the first-step energy-transfer probability  $K_1$  because the latter is necessary to populate the thulium  $^3F_4$  level, which is the ground state of the second ETU process, as shown in figure 4. We measured the  $^3H_4$  fluorescence emissions at 1500 nm under pumping at 975 nm.

Using filters with a bandwidth of 10 nm and centered at 1500 nm, we obtained the measurements shown in figure 5. The signal at 1500 nm is less intense than at 800 nm, but also less susceptible to re-absorption. The measured rise time is  $0.650 \pm 0.017$  ms.

### 2.3. Energy back-transfer process

The ytterbium back-transfer ( $K_5$ ) from the  $^3H_4$  thulium level to the  $^2F_{5/2}$  ytterbium level is explained in figure 6. Ytterbium

emission at 1064 nm under 795 nm pumping is shown in figure 7.

## 3. Rate equations

We used a numerical, time-resolved simulation which included all energy levels of figure 1. The system of eight differential, nonlinear equations is solved using a fourth-order Runge–Kutta algorithm. The parameters used for the numerical simulation are shown in table 1.

Given the pump beam spot size and the size of the laser beam within the crystal, as well as the respective beam quality  $M^2$  factors, the numerical simulation calculates the spatial overlap factors along the pump axis [12]:

$$\eta(z) = \sqrt{\frac{w_{Lx}^2(z)[w_{Lx}^2(z) + 2w_{Px}^2(z)]}{[w_{Lx}^2(z) + w_{Px}^2(z)]^2}} \times \sqrt{\frac{w_{Ly}^2(z)[w_{Ly}^2(z) + 2w_{Py}^2(z)]}{[w_{Ly}^2(z) + w_{Py}^2(z)]^2}} \quad (2)$$

where  $w_{Lx}$ ,  $w_{Ly}$  and  $w_{Px}$ ,  $w_{Py}$  are the laser and pump waists inside the crystal, respectively, perpendicular to the propagation axis  $z$ . The mode fill efficiency  $\eta_{mo}$  is the spatial overlap factor, weighted by the normalized pump absorption  $A \exp(-\alpha z)$ , where  $\alpha = \sigma_{36}n_3$  or  $\alpha = \sigma_{12}n_1$ , and integrated over the crystal length.

The rate equations for the population densities  $n_i$  and the photon density  $\phi$  are given by

$$\frac{dn_1}{dt} = -R_{12} + \frac{n_2}{\tau_2} + K_1 n_2 n_3 + K_2 n_2 n_4 + K_3 n_2 n_6 - K_5 n_1 n_6 \quad (3)$$

$$\frac{dn_2}{dt} = R_{12} - \frac{n_2}{\tau_2} - K_1 n_2 n_3 - K_2 n_2 n_4 - K_3 n_2 n_6 + K_5 n_1 n_6 \quad (4)$$

$$\frac{dn_3}{dt} = -R_{36} + \frac{n_4}{\tau_4} + \frac{\beta_{63}n_6}{\tau_6} + \frac{\beta_{73}n_7}{\tau_7} - K_1 n_2 n_3 - K_4 n_3 n_6 + K_5 n_1 n_6 \quad (5)$$

$$\frac{dn_4}{dt} = -\frac{n_4}{\tau_4} + \frac{n_5}{\tau_5} + \frac{\beta_{64}n_6}{\tau_6} + \frac{\beta_{74}n_7}{\tau_7} - K_2 n_2 n_4 + 2K_4 n_3 n_6 \quad (6)$$

$$\frac{dn_5}{dt} = R_{SE} - \frac{n_5}{\tau_5} + \frac{\beta_{65}n_6}{\tau_6} + \frac{\beta_{75}n_7}{\tau_7} + K_1 n_2 n_3 \quad (7)$$

$$\frac{dn_6}{dt} = R_{36} - R_{SE} - \frac{n_6}{\tau_6} + \frac{\beta_{76}n_7}{\tau_7} + K_2 n_2 n_4 - K_3 n_2 n_6 - K_4 n_3 n_6 - K_5 n_1 n_6 \quad (8)$$

$$\frac{dn_7}{dt} = -\frac{n_7}{\tau_7} + K_3 n_2 n_6 \quad (9)$$

$$\frac{d\phi}{dt} = \frac{L_{cr}}{L_{cav}} c N_0^{Tm} \left( R_{SE} + f_{geo} f_{UtoL} \frac{n_6}{\tau_6} \sigma_{em} \right) + \frac{\ln(R_{out}T) c \phi}{2L_{cav}} \quad (10)$$

where the energy levels are labeled as in figure 1, starting with the two ytterbium energy levels. Energy level 3 is the thulium ground level and energy level 6 is the thulium upper laser level for the 2.3  $\mu\text{m}$  emission. Since the  $^3F_2$  and  $^3F_3$  levels are thermally coupled to the  $^3H_4$  level, they are treated as one combined level 6.

The pump rates  $R_{12}$  and  $R_{36}$  are given by

$$R_{ij} = \phi_{ij} \eta_{deliv} \sigma_{ij} n_i \quad (11)$$

where the  $\sigma_{ij}$  are the effective pump absorption cross sections  $\sigma_{12}$  and  $\sigma_{36}$ , respectively, and  $\phi_{ij}$  is the photon pump rate per volume given by

$$\phi_{ij} = \frac{P_{ij} \lambda_{ij} \eta_{mo} \eta_{deliv}}{c h w_{Px} w_{Py}} \quad (12)$$

where  $\eta_{deliv}$  is pump delivery efficiency.

The stimulated emission rate is given by [13]

$$R_{SE} = \left( b_{ULL} n_6 - \frac{g_{ULL}}{g_{LLL}} b_{LLL} n_5 \right) \sigma_{em} \phi. \quad (13)$$

The geometrical fraction of the spontaneous emission is given by [14]

$$f_{geo} = \frac{w_{Lx} w_{Ly} \pi}{4\pi L_{cav}^2}. \quad (14)$$

**Table 1.** Parameters used in the numerical simulation.

Parameter	Value
Fluorescence lifetime $^2F_{5/2}$ ( $\tau_2$ )	$2 \times 10^{-3}$ s [9]
Fluorescence lifetime $^3F_4$ ( $\tau_4$ )	$15 \times 10^{-3}$ s [9]
Fluorescence lifetime $^3H_5$ ( $\tau_5$ )	$1 \times 10^{-6}$ s [9]
Fluorescence lifetime $^3H_4$ ( $\tau_6$ )	$1.2 \times 10^{-3}$ s [7]
Fluorescence lifetime $^1G_4$ ( $\tau_7$ )	$0.75 \times 10^{-3}$ s [9]
Transfer probability $K_1$	$649 \text{ s}^{-1}$ [9]
Transfer probability $K_2$	$3245 \text{ s}^{-1}$ [9]
Transfer probability $K_3$	$4000 \text{ s}^{-1}$ [9]
Transfer probability $K_4$	$500 \text{ s}^{-1}$ [9]
Transfer probability $K_5$	$210 \text{ s}^{-1}$ [9]
Branching ratio $^3H_4 \rightarrow ^3H_6$ ( $\beta_{63}$ )	0.924 [10]
Branching ratio $^1G_4 \rightarrow ^3H_6$ ( $\beta_{73}$ )	0.406 [10]
Branching ratio $^3H_4 \rightarrow ^3F_4$ ( $\beta_{64}$ )	0.07 [10]
Branching ratio $^1G_4 \rightarrow ^3F_4$ ( $\beta_{74}$ )	0.076 [10]
Branching ratio $^3H_4 \rightarrow ^3H_5$ ( $\beta_{65}$ )	0.006 [10]
Branching ratio $^1G_4 \rightarrow ^3H_5$ ( $\beta_{75}$ )	0.366 [10]
Branching ratio $^1G_4 \rightarrow ^3H_4$ ( $\beta_{76}$ )	0.155 [10]
Active center number density for 9.4 mol% Yb ( $n_{Yb}$ )	$13.4 \times 10^{20} \text{ cm}^{-3}$
Active center number density for 1.2 mol% Tm ( $n_{Tm}$ )	$1.6 \times 10^{20} \text{ cm}^{-3}$
Laser emission cross section ( $\sigma_{em}$ )	$1.2 \times 10^{-20} \text{ cm}^2$
Laser absorption cross section ( $\sigma_{ab}$ ) at 975 nm	$3.3 \times 10^{-21} \text{ cm}^2$
Effective pump absorption cross section at 960 nm and 25 °C ( $\sigma_{12}$ )	$7.0 \times 10^{-21} \text{ cm}^2$
Effective pump absorption cross section at 685 nm and 25 °C ( $\sigma_{36}$ )	$2.2 \times 10^{-20} \text{ cm}^2$
Upper laser level Boltzmann occupation factor ( $b_{ULL}$ )	0.19
Lower laser level Boltzmann occ. fac. (second highest Stark level of $^3H_5$ ) ( $b_{LLL}$ )	0.28
Degeneracy of upper laser level ( $g_{ULL}$ )	1 [11]
Degeneracy of lower laser level ( $g_{LLL}$ )	2 [11]
960 nm laser diode spot size at focus (horizontal $\times$ vertical)	$230 \times 230 \mu\text{m}^2$
$M^2$ pump beam parameter product (horizontal $\times$ vertical)	$42 \times 29$
Crystal length ( $L_{cr}$ )	4.6 mm
Cavity length ( $L_{cav}$ )	2 cm
960 nm nominal pump power ( $P_{12}$ )	20 W
685 nm nominal pump power ( $P_{36}$ )	5 W
OPO pump power at 960 and 780 nm	260 000 W
OPO pulse duration	4 ns
Pump delivery efficiency ( $\eta_{deliv}$ )	0.61
Mode fill efficiency ( $\eta_{mo}$ )	0.77
Cavity loss	0.99
Output mirror reflectivity ( $R$ )	0.988
Fraction of spontaneous emission coupled into laser mode ( $f_{geo}$ )	$1.6 \times 10^{-5}$
Radiatively emitted decay rate from upper laser level to lower laser level ( $f_{UtoL}$ )	$0.006 \text{ s}^{-1}$

The output power of the laser is calculated by

$$P_{OUT} = \frac{(1 - R_{out})}{2} \phi \frac{hc}{\lambda_L} w_x w_y. \quad (15)$$

#### 4. Laser experiments

The same crystal used for the OPO measurements was end-pumped by a 20 W, 960 nm diode bar that was focused at the

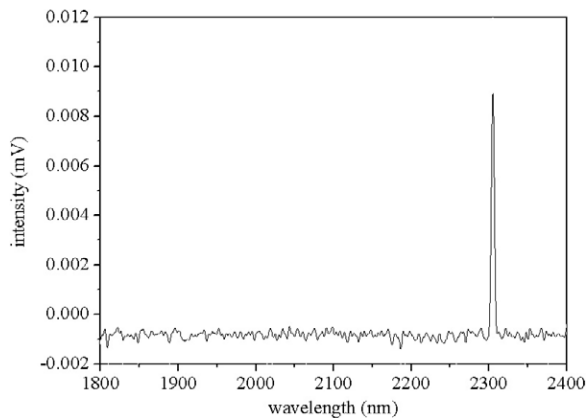


Figure 8. Laser output spectrum.

Brewster cut crystal of 4.6 mm length inside the hemispherical cavity of 1% output transmission. For the end-pumping setup, a series of lenses and a two-mirror beamshaper were used to reconfigure the diode emission into a more circular beam with approximately equal  $M^2$  factors in the  $x$ - and  $y$ -directions [15]. A pump intensity of  $19 \text{ kW cm}^{-2}$  and an  $M^2$  quality factor of  $42 \times 29$  (horizontal  $\times$  vertical) were used at the crystal position as measured with a calibrated power meter and a CCD, using the second-moment method to calculate the beam spot sizes. The pump spot size was  $230 \times 230 \mu\text{m}^2$ . The temporal behavior of the output pulse was analyzed with a thermoelectrically cooled InAs detector. Due to losses in the beamshaper and the input mirror, the maximum pump power was 11 W. A maximum of 620 mW of  $2.3 \mu\text{m}$  laser radiation was achieved (see figure 8) in a quasi-continuous operation (8 ms pulses, 10 Hz) using 960 nm pump radiation only. Lasing at the  $2 \mu\text{m}$  ground-level transition is not possible in this system with low  $\text{Tm}^{3+}$  concentration and Yb co-doping [9]. The main reason is that the  $\text{Tm}^{3+}$  ground state cannot be depleted due to the relative small rates  $K_1$  and  $K_4$ . Additionally, the upper laser level for the  $2 \mu\text{m}$  transition is depleted by the second ETU process.

In the double pumping configuration, a 5 W diode bar at 685 nm is used, as shown in figure 9. For the 685 nm, side-pumped setup, a half-wave plate was used to rotate the diode's emission parallel to the crystal's  $c$ -axis in order to access its high absorption coefficient of  $4.3 \text{ cm}^{-1}$  (1 mol% doping). The pump beam was incident on the top surface of the crystal. A 3 cm spherical lens and mirror at  $45^\circ$  matched the pump beam to the laser mode size inside the crystal. Due to losses, the maximum pump power was 4.5 W. An indium foil between the crystal and the heat-sink reflected the 685 nm pump beam back into to the laser mode. A total absorbed pump power of 600 mW was estimated in this double-pass, side-pumped configuration. In order to allow the 685 nm pump beam to access the crystal from the top it was not possible to remove the generated heat from the crystal's top face, and therefore, quasi-continuous wave operation had to be employed. Pulse durations ranged from 2 to 10 ms at 10 to 40 Hz.

Pump power and output power measurements were done with a calibrated power meter of 10 mW resolution

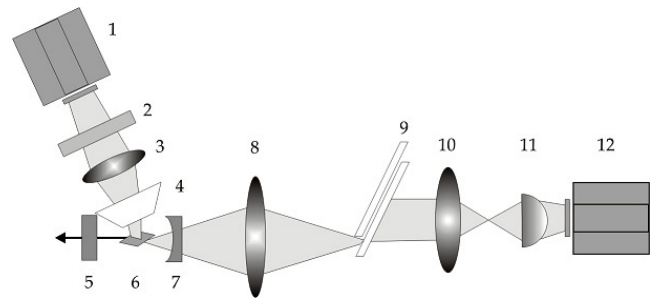


Figure 9. Pumping scheme: (1) 685 nm diode laser; (2)  $\lambda/2$  waveplate; (3) spherical lens; (4) folding mirror; (5) output coupler; (6) Brewster cut Yb:Tm:YLF crystal; (7) input mirror; (8) spherical lens; (9) two-mirror beamshaper; (10) spherical lens; (11) cylindrical lens; (12) 960 nm diode laser.

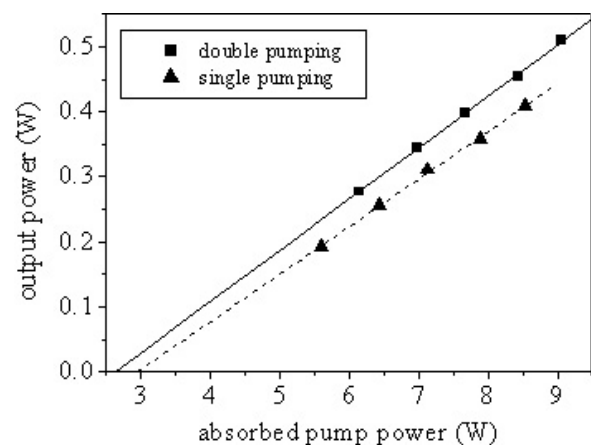
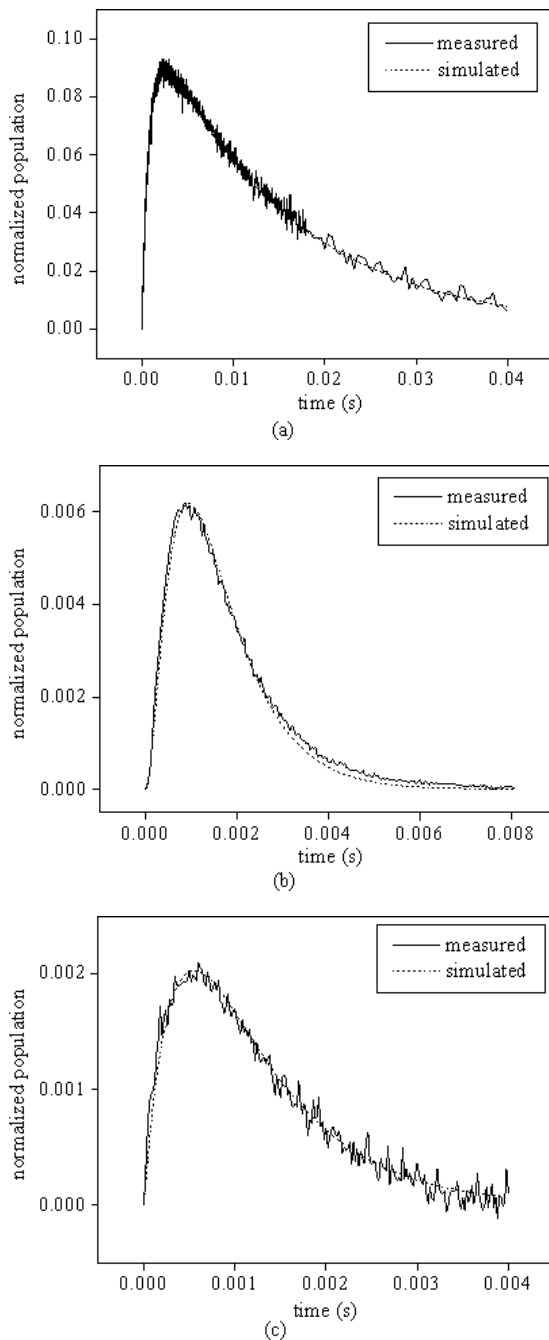


Figure 10. Output power of the Yb:Tm:YLF laser at  $2.3 \mu\text{m}$  as a function of input power for single-pumping and double-pumping schemes.

(NEWPORT 818T-150). Diode emission spectra were recorded with a portable spectrometer (HR2000, USBio Solutions Inc.), with 0.11 nm resolution. Crystal absorption and emission spectra were recorded with a high-resolution spectrometer (Cary 13D). The effective pump absorption cross sections,  $\sigma_{12}$  and  $\sigma_{36}$ , are given by the overlap of the respective normalized diode emission spectra and the crystal absorption spectra, integrated over the crystal length  $L_{\text{cr}}$ . The temporal behavior of the output pulse was analyzed with a thermoelectrically cooled, fast rise time ( $< 2 \text{ ns}$ ), InAs detector (Virgo System InAs-PVI-2TE), coupled to a 20 MHz preamplifier (Virgo VPDC-201). The pulses were recorded with digital storage oscilloscope (Tektronix TDS 360). Care was taken to attenuate the pulses in order to avoid saturation effects of the detector. Pump beam parameters were measured with a CCD coupled to a PC and dedicated software (WinCam; Merchantek Inc).

With 685 nm pumping only no laser action could be achieved. Slope efficiencies of  $7.3 \pm 0.15\%$  and  $7.9 \pm 0.15\%$  were obtained for single pumping at 960 nm and double pumping at 960 nm and 685 nm, respectively. In all cases the laser output beam was in  $\text{TEM}_{00}$  mode with an  $M^2$  beam quality factor of approximately  $1.3 \times 1.4$  in the vertical and



**Figure 11.** (a)–(c) Measured and simulated decay curves of the  $^3F_4$ ,  $^3H_4$  and  $^2F_{5/2}$  levels, respectively.

horizontal directions, respectively, as measured with the knife edge method. For the double-pumping scheme, the 685 nm diode is fixed at 5 W output power and only the 960 nm pump is varied. In figure 10 the output power is illustrated for an output coupler reflectance of 98.8% as a function of the total absorbed pump power. The threshold pump power reduced from 3.0 to 2.6 W for dual pumping, although care must be taken with this information, because a large error margin is involved in the estimate of the absorbed 685 nm pump power. Nevertheless, the slope of the two curves is statistically significantly different ( $p < 0.05$ ). Another interesting characteristic of the double-pumping scheme is that the laser turn-on time reduces from

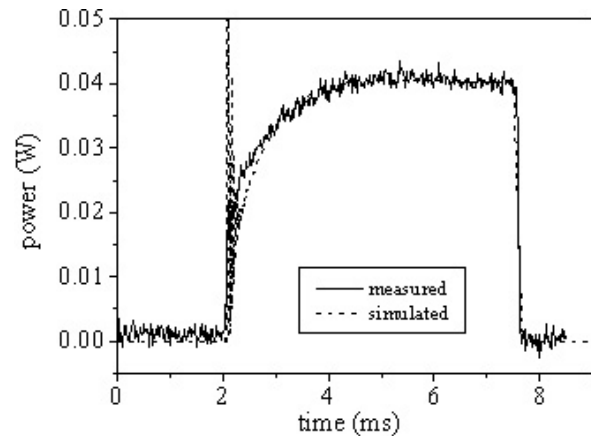


**Figure 12.** Measured and simulated output power curves obtained at low pump power (5 W).

1.0 ms in the single-pumping scheme to 0.82 ms in the double-pumping scheme. Because the resonator losses are the same in both cases, this demonstrates a higher small signal gain when using 685 nm. The additional 685 nm pump power clearly increases the slope efficiency.

### 5. Validation of the numerical simulation

The acquired spectra and the output power pulse of the laser were fitted with the above rate equations (figures 11 and 12). The only adjustable parameters are the cavity losses and the pump power. These parameters had to be adjusted very carefully in order to achieve a good fit.

The losses used in the simulation to achieve the fit of figure 12 are 0.989 and the pump power used was 4.9 W. We did a Findlay–Clay analysis of the cavity losses with three different output coupling mirrors, and calculated  $0.021 \pm 0.011$  in agreement with the simulated loss.

### 6. Numerical simulation

#### 6.1. Pump absorption saturation at 685 nm

In order to understand why no laser action is seen under pure 685 nm pumping, the laser cavity was simulated with only the 685 nm radiation switched on and without the 960 nm pump. From figure 13 it can clearly be seen that a very high threshold pump power of approximately 5.5 W is necessary for laser action. This threshold pump power is higher than our available 5 W. The high threshold is due to the inefficient 685 nm side-pumping scheme.

Also clearly seen is the bottle-neck effect of the  $^3F_4$  energy level under 685 nm pumping that leads to a saturation of the absorption. The dotted line demonstrates what would happen if the  $^3F_4$  level lifetime were 1 ms and not 15 ms: it can be seen that the saturation behavior of the absorption is removed.

#### 6.2. Optimized values of 685–960 nm pump power ratio

For the cavity described in figure 9 and the parameters used in table 1, the simulation demonstrates that the optimum fraction

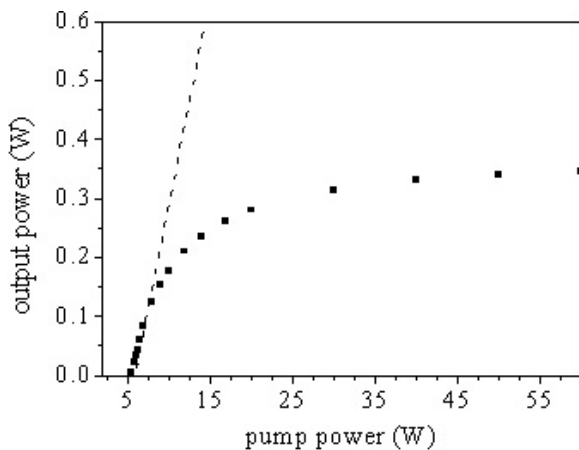


**Figure 13.** Numerical simulation of the output power as a function of 685 nm pump power (squares). The dashed line is a simulation using an imaginary lifetime of 1 ms for the  $^3F_4$  level.

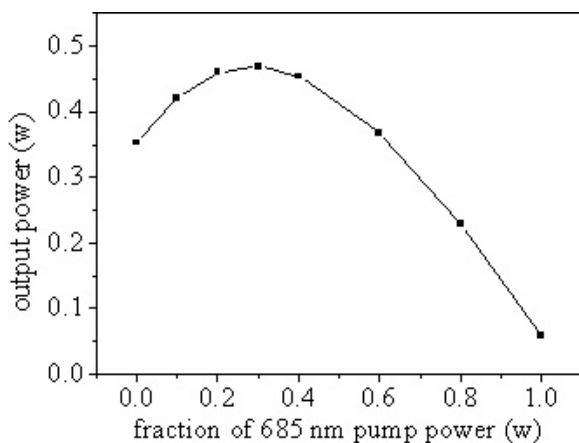


**Figure 14.** Numerical simulation of the output power as a function of the fraction of 685 nm pump power maintaining a total input power of 12 W.

of 685 nm pump power is about 35% (shown in figure 14). This generates a significant increase in output power of almost 33%. It should be remarked that the optimum fraction of 685 nm pump power is a function of pump absorption efficiency and therefore depends on the pump parameters as well as crystal doping and geometry. The simulation also demonstrates clearly that pure 685 nm pumping is inefficient due to the bottle-neck effect of the  $^3F_4$  energy level.

## 7. Conclusions

Yb:Tm:YLF laser operation at 2.3  $\mu\text{m}$ , achieved by pumping simultaneously at 685 and 960 nm, is demonstrated. The output power of 620 mW is, to our knowledge, the highest reported so far. Higher slope efficiency is achieved for double pumping with 685 nm, and an increase in output power of more than 30% seems possible if a total pump power fraction of 35% 685 nm pump radiation is used. The rate-equation model shows a good agreement between numerical simulation and experimental data for a diode-pumped Yb:Tm:YLF laser emitting at 2.3  $\mu\text{m}$ .

## Acknowledgments

We would like to thank the National Science Council (CNPq) and the State Foundation for Research (FAPESP) for the financial support of this work.

## References

- [1] McAleavey F J, O’Gorman J, Donegan J F, Hegarty J and Maze G 2001 *Sensors Actuators A* **87** 107
- [2] Cerutti L, Garnache A, Ouvrard A, Garcia M and Genty F 2005 *Phys. Status Solidi a* **2002** 631
- [3] Webber M E, Wang J, Sanders S T, Baer D S and Hanson R K 2000 *Proc. Combust. Inst.* **28** 407
- [4] Olesberg J T, Mermelstein C, Schmitz J and Wagner J 2005 *Optical Diagnostics and Sensing V: Proc. SPIE* vol 5702 ed A V Priezzhev and G L Cote (Bellingham, WA: SPIE) pp 23–9
- [5] Pinto J F, Esterowitz L and Rosenblatt G H 1994 *Opt. Lett.* **19** 683
- [6] Sudesh V and Goldys E M 2000 *J. Opt. Soc. Am. B* **17** 1068
- [7] Braud A, Girard S, Doualan J L, Thuau M, Moncorgé R and Tkachuk A M 2000 *Phys. Rev. B* **61** 5280
- [8] da Vila L D, Gomes L, Tarelho L V G, Ribeiro S J L and Messaddeq Y 2004 *J. Appl. Phys.* **95** 5451
- [9] Dening A, Möbert P E A and Huber G 1998 *J. Appl. Phys.* **84** 5900
- [10] Razumova I K, Tkachuk A M, Mironov D I and Nikichev A A 1996 *Opt. Spectrosc.* **81** 205
- [11] Kaminskii A A 1981 *Laser Crystals: Their Physics and Properties (Springer Series in Optical Sciences vol 14)* (Berlin: Springer)
- [12] Clarkson W A and Hanna D C 1989 *J. Mod. Opt.* **36** 483
- [13] Pollnau M, Graf T, Balmer J E, Lüthy W and Weber H P 1994 *Phys. Rev. A* **49** 3990
- [14] Silfvost W T 1996 *Laser Fundamentals* (Cambridge: Cambridge University Press) p 214
- [15] Wetter N U, de Matos P S F, Ranieri I M, Courrol L C and Morato S P 2002 *Opt. Commun.* **204** 311